Newcastle Disease Virus Manipulates Mitochondrial MTHFD2-Mediated Nucleotide Metabolism for Virus Replication

Ning Tang,[a,b] Pingyi Chen,[c] Changrun Zhao,[a] Panrao Liu,[d] Lei Tan,[b] Cuiping Song,[b] Xusheng Qiu,[b] Ying Liao,[b] Xiufan Liu,[d] Tingrong Luo,[a,e] ⓘ Yingjie Sun,[b] ⓘ Chan Ding[a,b,d]

aLaboratory of Veterinary Microbiology and Animal Infectious Diseases, College of Animal Sciences and Veterinary Medicine, Guangxi University, Nanning, Guangxi, China

bDepartment of Avian Infectious Diseases, Shanghai Veterinary Research Institute, Chinese Academy of Agricultural Science, Shanghai, P. R. China

cState Key Laboratory of Cellular Stress Biology, Innovation Center for Cell Signaling Network, School of Life Sciences, Xiamen University, Xiamen, P. R. China

dJiangsu Co-innovation Center for Prevention and Control of Important Animal Infectious Diseases and Zoonoses, College of Veterinary Medicine, Yangzhou University, Yangzhou, P. R. China

eState Key Laboratory for Conservation and Utilization of Subtropical Agro-Bioresources, Guangxi University, Nanning, Guangxi, China

ABSTRACT Viruses require host cell metabolic reprogramming to satisfy their replication demands; however, the mechanism by which the Newcastle disease virus (NDV) remodels nucleotide metabolism to support self-replication remains unknown. In this study, we demonstrate that NDV relies on the oxidative pentose phosphate pathway (oxPPP) and the folate-mediated one-carbon metabolic pathway to support replication. In concert with $[1,2\text{-}^{13}C_2]$ glucose metabolic flow, NDV used oxPPP to promote pentose phosphate synthesis and to increase antioxidant NADPH production. Metabolic flux experiments using $[2,3,3\text{-}^2H]$ serine revealed that NDV increased one-carbon (1C) unit synthesis flux through the mitochondrial 1C pathway. Interestingly, methylenetetrahydrofolate dehydrogenase (MTHFD2) was upregulated as a compensatory mechanism for insufficient serine availability. Unexpectedly, direct knockdown of enzymes in the one-carbon metabolic pathway, except for cytosolic MTHFD1, significantly inhibited NDV replication. Specific complementation rescue experiments on small interfering RNA (siRNA)-mediated knockdown further revealed that only a knockdown of MTHFD2 strongly restrained NDV replication and was rescued by formate and extracellular nucleotides. These findings indicated that NDV replication relies on MTHFD2 to maintain nucleotide availability. Notably, nuclear MTHFD2 expression was increased during NDV infection and could represent a pathway by which NDV steals nucleotides from the nucleus. Collectively, these data reveal that NDV replication is regulated by the c-Myc–mediated 1C metabolic pathway and that the mechanism of nucleotide synthesis for viral replication is regulated by MTHFD2.

IMPORTANCE Newcastle disease virus (NDV) is a dominant vector for vaccine and gene therapy that accommodates foreign genes well but can only infect mammalian cells that have undergone cancerous transformation. Understanding the remodeling of nucleotide metabolic pathways in host cells by NDV proliferation provides a new perspective for the precise use of NDV as a vector or in antiviral research. In this study, we demonstrated that NDV replication is strictly dependent on pathways involved in redox homeostasis in the nucleotide synthesis pathway, including the oxPPP and the mitochondrial one-carbon pathway. Further investigation revealed the potential involvement of NDV replication-dependent nucleotide availability in promoting MTHFD2 nuclear localization. Our findings highlight the differential dependence of NDV on enzymes for one-carbon metabolism, and the unique mechanism of action of MTHFD2 in viral replication, thereby providing a novel target for antiviral or oncolytic virus therapy.

Address correspondence to Tingrong Luo, tingrongluo@gxu.edu.cn, Yingjie Sun, sunyingjie@shvri.ac.cn, or Chan Ding, shoveldeen@shvri.ac.cn.

Oncolytic viral therapy is a promising treatment modality for a variety of malignancies (1). Newcastle disease virus (NDV), which belongs to the *Paramyxoviridae* family, is a natural oncolytic virus that selectively infects and replicates in tumor cells, thereby providing a method for killing tumor cells (2). For effective replication, NDV tends to hijack various tumor cell metabolic pathways to obtain the nucleotides, amino acids, energy, and other substances required for virus replication. Nucleotides are intricately involved in tumor development and virus replication; therefore, targeting the nucleotide synthesis pathway has become an area of keen research interest in the development of antitumor and antiviral therapies (3, 4). Antiviral studies targeting nucleotides have focused on the pentose phosphate pathway (PPP) and folate-mediated one-carbon (1C) metabolism pathway, as these pathways provide indispensable substrates for nucleotide synthesis (5). However, the mechanism by which oncolytic viruses hijack these specific pathways for efficient replication remains unclear.

Nucleotide synthesis relies on glucose to provide a variety of precursors, including phosphoribosyl diphosphate (PRPP), serine, and glycine, through the PPP and 1C metabolic pathways. As an important branch of the glycolytic pathway, the PPP generates PRPP for nucleotide synthesis, as well as NADPH to maintain intracellular redox homeostasis (6). Interestingly, the upregulation of glycolytic intermediate metabolites is beneficial for nucleotide synthesis via the nonoxidative PPP (7, 8). Previous studies have shown that NDV extensively reshapes carbohydrate metabolism and increases the levels of intracellular reactive oxygen species (ROS) (9). In response to induced oxidative stress, the oxidative PPP (oxPPP) (10) and the 1C metabolism (11) pathways may become the preferred pathways for hijacking by the virus due to their ability to generate NADPH for antioxidant use and nucleotide precursors for nucleotide synthesis.

NADPH is also generated to maintain the intracellular redox balance during folate-mediated one-carbon metabolism, which generates and transfers 1C units for nucleotide synthesis via the cytosolic SHMT1 and mitochondrial SHMT2-MTHFD2 pathways (12). A deficiency in SHMT creates a state of metabolic redox imbalance and primarily reduces the contribution of 5,10-methylene-tetrahydrofolate (5,10-meTHF) to downstream metabolic reactions (13–15). Cytosolic methylene tetrahydrofolate dehydrogenase 1 (MTHFD1) participates in redox homeostasis by catalyzing the synthesis of 10-formyl-THF from formate for purine synthesis and consuming the intracellular antioxidant NADPH. Therefore, deletion of MTHFD1 suppresses viral replication (16). Cytosolic methylene tetrahydrofolate dehydrogenase 1 (MTHFD1) participates in redox homeostasis by catalyzing the synthesis of 10-formyl-THF from formate for purine synthesis and consuming the intracellular antioxidant NADPH. Therefore, deletion of MTHFD1 suppresses viral replication (17, 18) and decreases formate-driven purine synthesis by blocking mitochondrial formate generation and transport to the cytosolic 1C pool (19). Notably, the regulation of mitochondrial one-carbon metabolic pathways by inhibitors, such as c-Myc, leads to an increased production of glycine and 1C units in response to cellular proliferation (18, 20). Interestingly, increases in the nuclear expression of MTHFD2 in proliferating cells can promote DNA replication (21) or prevent DNA damage (19). Therefore, MTHFD2 may have a unique function that is distinct from other one-carbon metabolic enzymes.

Here, we compare the dependence of NDV replication on the cytosolic and mitochondrial pathways of 1C metabolism. In brief, we found that NDV selectively increases 1C unit synthesis via the mitochondrial 1C pathway and increases mitochondrial MTHFD2 expression in response to a lack of available serine. The finding that MTHFD2 is the target by which NDV hijacks the mitochondrial 1C metabolic pathway for nucleotide synthesis is particularly interesting. NDV replication depends on MTHFD2 to maintain the cellular redox balance and promotes MTHFD2 expression in the nucleus to perform nonenzymatic functions. Treatment of NDV-infected cells lacking SHMT2 or MTHFD1L of the mitochondrial pathway with formate or extracellular nucleotides fails to restore NDV replication. Thus, NDV replication depends on the mitochondrial pathway of 1C metabolism to provide 1C
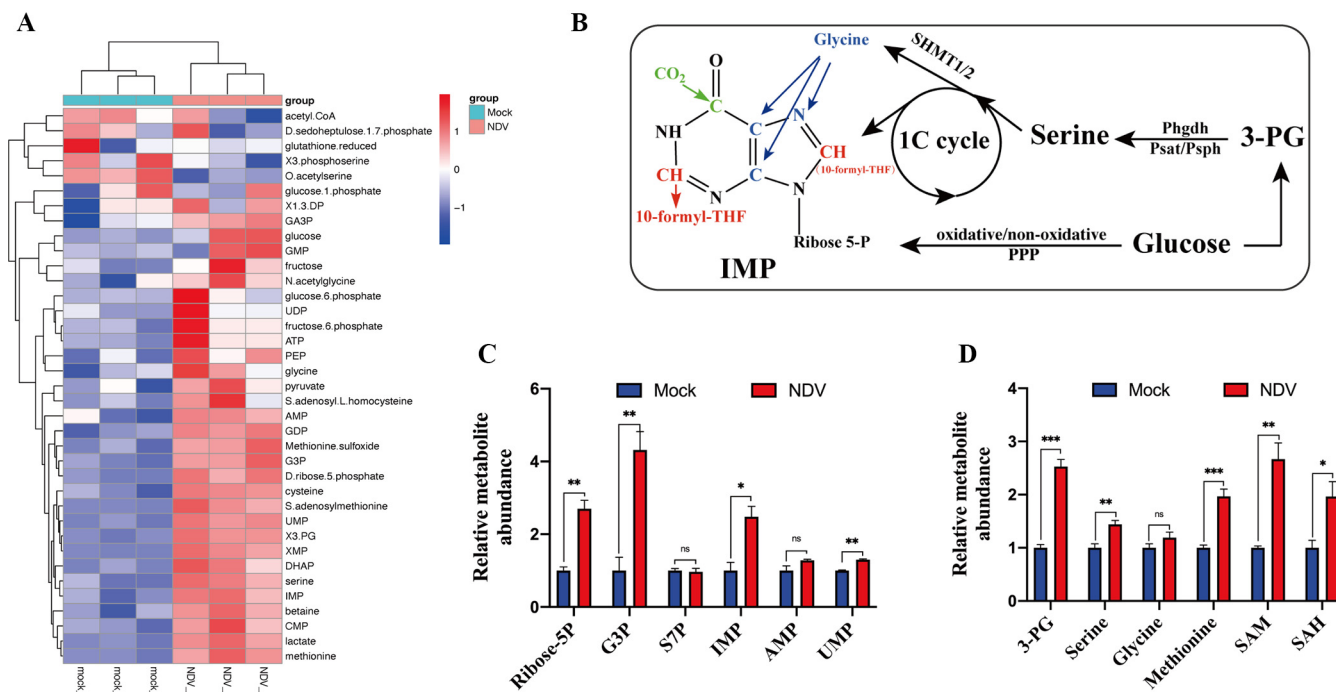
FIG 1 NDV infection upregulated intermediate metabolites in a variety of metabolic pathways associated with nucleotide synthesis. (A) Heat map for a comparative analysis of differential intracellular metabolites after 12 h treatment with NDV-infected cells versus uninfected cells. (B) Precursors of hypoxanthine nucleotides synthesis and their anabolic pathways. (C) Comparative analysis of metabolites associated with the pentose phosphate pathway and nucleotides in infected versus uninfected cells. (D) Intracellular metabolites of the *de novo* serine synthesis pathway and one-carbon metabolism in infected versus uninfected cells. ns, not significant; *, $P < 0.05$; **, $P < 0.01$; ***, $P < 0.001$ by a two-sample t test. Data are presented as the mean $\pm$ standard deviation (SD); $n = 3$ independent biological replicates.

units for nucleotide biosynthesis and to generate NADPH to maintain the cellular redox balance.

RESULTS

Glycolytic and one-carbon metabolic pathways were enriched by NDV infection. Alterations in intracellular metabolite concentrations indirectly reflect relevant metabolic pathways that may be hijacked by viral replication (5). We identified virus-induced intracellular nucleotide-related metabolic pathways important for NDV replication by liquid chromatography-mass spectrometry (LC-MS) examination of intermediates of glycolysis, the PPP, and the 1C metabolic pathway in NDV-infected cells. A heatmap indicated significant upregulation of metabolites associated with nucleotide metabolic pathways by NDV infection (Fig. 1A). As shown in Fig. 1B, the *de novo* synthesis of IMP requires a variety of precursors, with the PPP providing ribose 5-phosphate and serine acting as the donor of 1C units for folate-mediated 1C metabolism. Numerous studies have shown that the PPP and 1C metabolic pathways are targets for both antitumor and virus treatments (10, 22). In the present study, the levels of metabolic intermediates in the nucleotide synthesis pathway, including ribose 5-phosphate (R5P), glyceraldehyde 3-phosphate (G3P), IMP, and UMP, were increased in NDV-infected cells (Fig. 1C). Of these, G3P can interact with sedoheptulose-7-phosphate (S7P) to form R5P through the nonoxidative PPP (8). The 1C folate cycle mediates serine catabolism to generate 1C units to support DNA and RNA biosynthesis. NDV infection upregulated 3-phosphoglycerate (3-PG), serine, and glycine levels above those seen in uninfected cells (Fig. 1D), and the accumulation of 3-PG led to the upregulation of *de novo* serine synthesis (23). NDV also upregulated the methionine cycle metabolites S-adenosylmethionine (SAM) and S-adenosylhomocysteine (SAH) (Fig. 1D), which are primarily important in DNA and protein methylation reactions. Our findings showed that NDV significantly disrupted intracellular nucleotide metabolic pathways, suggesting that PPP and serine metabolism may serve as targets for inhibiting NDV replication.
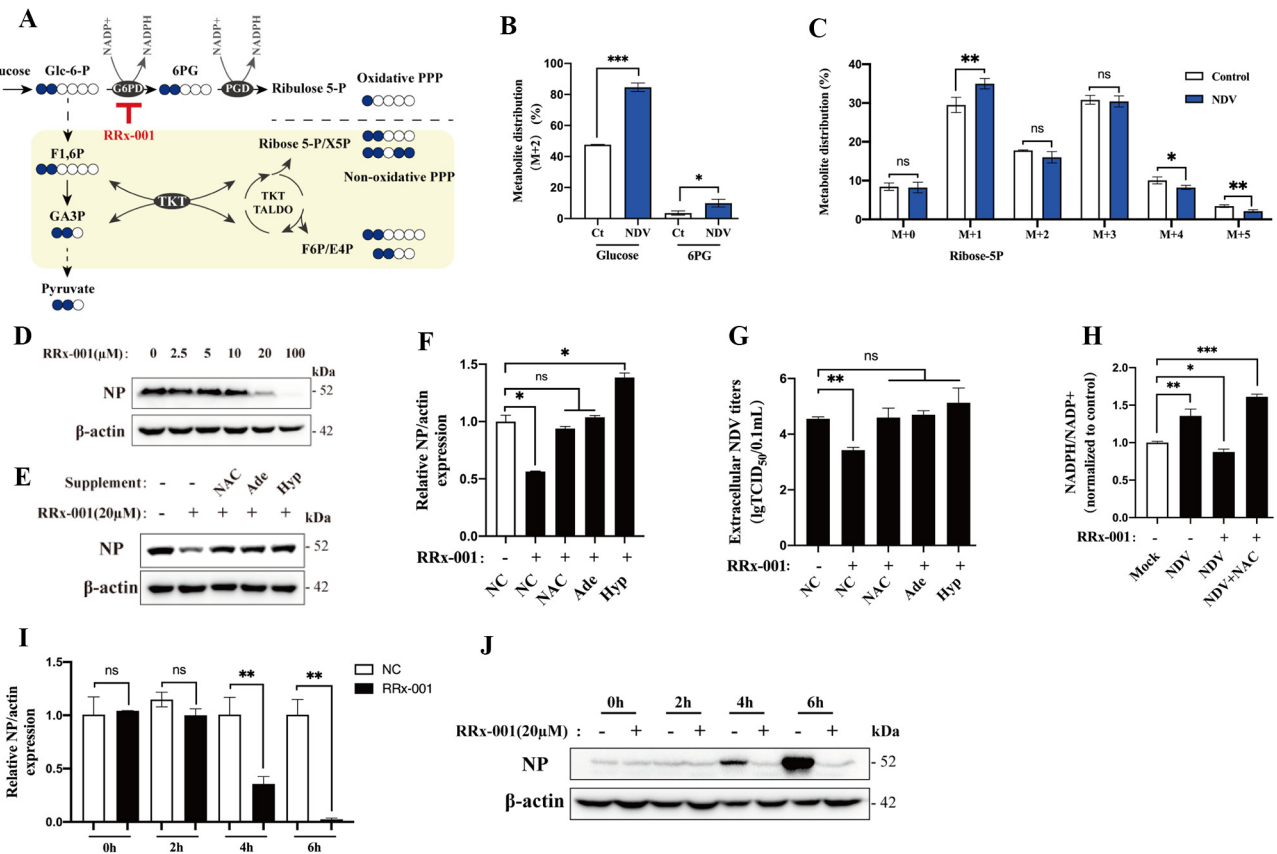
FIG 2 NDV replication selectively activates the oxPPP to maintain redox homeostasis and promote nucleotide synthesis. (A) Schematic of the [1, 2-^{13}C$_2$] glucose metabolic flux in the pentose phosphate, glycolysis, and *de novo* serine synthesis pathways and the target of RRx-001. (B) Proportion of the total pool of 6PG (M + 2) originating from [1, 2-^{13}C$_2$] glucose and glucose (M + 2) uptake induced by NDV. (C) NDV drives [1, 2-^{13}C$_2$] glucose metabolism to produce the oxidized (M + 1) and reduced (M + 2) forms of ribose-5P by the pentose phosphate pathway. (D) Western blot analysis of NDV NP expression in infected cells treated with increasing amounts of RRx-001 for 12 h. NDV NP protein expression (E) and relative NDV NP expression levels were normalized to β-actin (F), and the extracellular NDV titers (G) were determined during RRx-001 inhibition of NDV replication by supplementation with NAC (1.0 μM), adenine (Ade) (25 μM), and hypoxanthine (Hyp) (6 μM). (H) Intracellular NADPH/NADP$^+$ ratios were measured after treatment with RRx-001 or supplementation with NAC (final concentration, 1.0 μM) for 12 h. Effect of RRx-001 pretreatment on NDV adsorption to cells by detection of the NDV NP mRNA transcript levels (I) and protein levels (J). ns, not significant; *, $P < 0.05$ and ***, $P < 0.001$ by a two-sample t test. Data are presented as the mean $\pm$ SD; $n = 3$ independent biological replicates.

Selective activation of oxPPP by NDV infection promotes antioxidant defenses and nucleotide synthesis. Glycolysis has previously been demonstrated as essential for NDV replication (9). As an important branch of glycolysis, the PPP is essential for cellular proliferation (24) and relies on an oxidative or nonoxidative pathway to generate R5P for nucleotide synthesis (7, 25). We further investigated whether the oxidative or the nonoxidative PPP was remodeled under NDV infection by exposing infected and uninfected cells to [1,2-^{13}C$_2$] glucose medium for 12 h. Figure 2A presents a schematic diagram of our [1,2-^{13}C$_2$] stable isotope glucose-labeling experiments. The operation of the oxidative or nonoxidative pathways can be determined by the R5P labeling pattern of the metabolites in the infected cells. The isotope tracing experiments showed that NDV infection increased glucose (M + 2) uptake as well as the metabolic flux of glucose conversion to 6PG (M + 2) in the PPP (Fig. 2B). NDV also significantly increased the flux of R5P through oxidative PPP (M + 1) compared to that of the uninfected group (Fig. 2C). By contrast, the synthesis flux through the nonoxidative pathway (M + 2) was not affected by virus infection (Fig. 2C), consistent with the nonsignificant change in S7P determined by metabolomics analysis (Fig. 1C). The increased glucose flux into the PPP through the oxidative pathway facilitates viral replication and increases antioxidant capacity (10, 24). Our findings indicate that NDV replication may be selectively dependent on the oxidative PPP.

We verified NDV-induced oxidative PPP as a restrictive target for viral replication by treating NDV-infected cells with RRx-001, a selective inhibitor of glucose 6-phosphate dehydrogenase

(G6PD), the rate-limiting enzyme of the oxidative PPP (Fig. 2A). RRx-001 treatment significantly and dose-dependently reduced NDV NP protein expression (Fig. 2D). We further determined whether the block of NDV replication was due to a disruption of redox homeostasis or insufficient PPP-mediated nucleotide synthesis by adding exogenous antioxidants and nucleotides in rescue experiments. Figure 2E shows that supplementation of RRx-001-treated infected cells with N-acetylcysteine (NAC) (a precursor of GSH synthesis), exogenous adenine (Ade), and hypoxanthine (Hyp) could rescue viral replication. NP gene expression in infected cells and the virus titer in the extracellular medium were consistent with the Western blotting results (Fig. 2F and G). NAC supplementation increased the intracellular $NADPH/NADP^+$ ratio, which is beneficial for DNA synthesis (26). The NDV-infected cells showed an increase in the intracellular $NADPH/NADP^+$ ratio, RRx-001 treatment reduced the $NADPH/NADP^+$ ratio, and NAC treatment restored this ratio (Fig. 2H). These findings indicated that NAC treatment could restore the redox balance disrupted by RRx-001 to promote nucleotide synthesis. We verified whether RRx-001 affected the adsorption of NDV to the cells by treating the cells with RRx-001 3 h before NDV infection. Figure 2I and J show that this pretreatment did not affect the adsorption of NDV but significantly inhibited the transcription level of the virus. Collectively, these results suggest that NDV replication depends on oxPPP-driven nucleotide synthesis and antioxidant activity.

NDV replication can tolerate serine deficiency and selects the mitochondrial pathway to produce 1C units. Oxidative PPP-mediated nucleotide synthesis requires R5P as well as 1C units produced by serine catabolism (27); therefore, we determined the role of serine catabolism in the process of NDV replication. As an intermediate metabolite of the glycolysis pathway, 3-PG is also the source of the carbon skeleton for *de novo* serine synthesis (Fig. 3A). Although 3-PG was upregulated by NDV infection (Fig. 1C), the metabolic flux of $[1,2-^{13}C_2]$ glucose conversion to serine (M + 2) was decreased (Fig. 3B). We examined the dependence of NDV replication on *de novo* serine synthesis by treating cells with the inhibitor, NCT-503, or small interfering RNA (siRNA) that targeted PHGDH activity and then assessing intracellular NDV replication by the accumulation of NDV NP observed by Western blotting. Surprisingly, intracellular NDV NP expression was not significantly affected by these treatments (Fig. 3C and D), indicating that NDV replication was independent of *de novo* serine synthesis. Therefore, we speculated that NDV replication was dependent on serine derived from extracellular uptake. To confirm this, we cultured NDV-infected cells in serine-deficient medium and analyzed them at different times. Western blots showed that serine depletion inhibited NDV replication only in the early stages of replication (Fig. 3E). Interestingly, only MTHFD2, among the folate-mediated 1C metabolic enzymes, was significantly upregulated by serine deficiency (Fig. 3E and F). Similar results were obtained in NDV-infected cells treated with NCT-503, which blocked serine synthesis but promoted a compensatory upregulation of MTHFD2 (Fig. 3G and H). Serine deficiency-induced accumulation of MTHFD2 can be recapitulated in infected Beas-2B cells (see Fig. S1B in the supplemental material). These findings suggested that MTHFD2 may play a compensatory role in serine deficiency.

Serine taken up by cells can be catabolized into glycine and dTMP by cytosolic and mitochondrial 1C pathways. We used isotope tracing experiments to identify which 1C metabolic pathway was activated by NDV infection by exposing infected and uninfected cells to $[2,3,3-^2H]$-serine. The labeled $[2,3,3-^2H]$-serine was catabolized to form a deuteron-containing glycine (M + 1), whereas another product, dTMP, was formed via the cytosolic and mitochondrial pathways to form labeled M + 2 and M + 1, respectively (Fig. 3I). Increased uptake of $[2,3,3-^2H]$-serine was observed following NDV infection (Fig. 3J), and the proportions of labeled glycine and dTMP were slightly increased compared to the uninfected cells (Fig. 3K and L). NDV appeared to upregulate mitochondrial MTHFD2 expression as a compensatory response to serine deficiency, indicating that NDV may utilize the mitochondrial 1C pathway to support viral replication. Overall, NDV replication appeared to be independent of *de novo* serine synthesis, but 1C metabolism had an important function in NDV replication.

One-carbon metabolism emerges as a critical target for NDV replication. Folate-mediated 1C metabolism involves the following two parallel metabolic reactions: (i) one in the cytosolic SHMT1-MTHFD1 pathway, and (ii) one in the mitochondrial SHMT2-MTHFD2-MTHFD1L pathway. Serine deficiency upregulated the key mitochondrial enzyme that
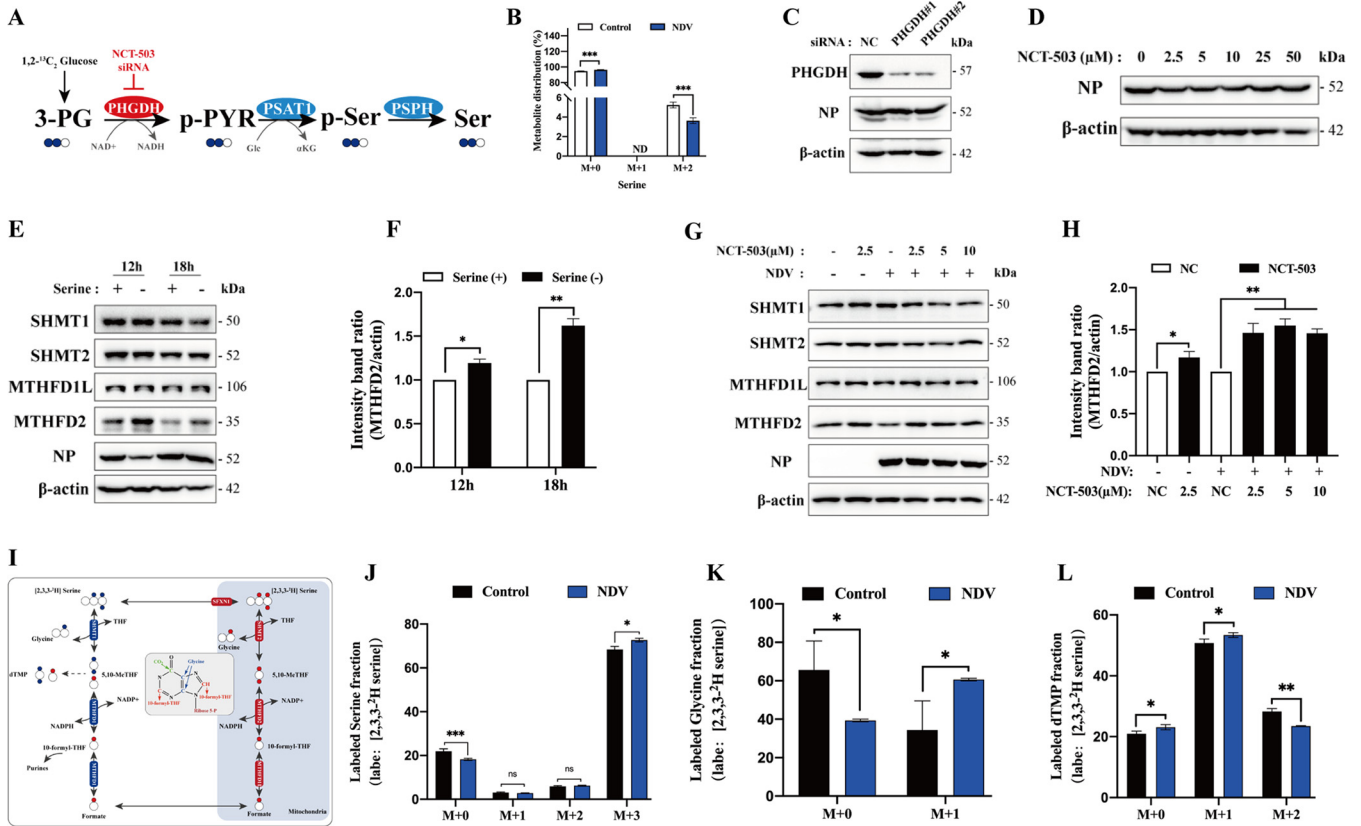
FIG 3 NDV increases 1C unit synthesis via the mitochondrial 1C pathway but independently the *de novo* serine synthesis pathway. (A) Schematic of [1, 2-$^{13}C_2$] glucose metabolic flux in *de novo* serine synthesis pathway and target of NCT-503 and siRNA. (B) Contribution of [1, 2-$^{13}C_2$] glucose to serine (M + 2) synthesis induced by NDV infection. (C) Effect of siRNA interference of PHGDH expression on NDV NP protein expression. (D) Western blot analysis of NDV NP expression in infected cells treated with increasing amounts of NCT-503 for 12 h. (E and F) Effect of serine depletion on NDV NP protein expression and folate-mediated one-carbon metabolic enzyme in infected cells. (G and H) Effect of NCT-503 targeting PHGDH to block the *de novo* serine synthesis pathway on the expression of NDV NP and folate-mediated one-carbon metabolic enzyme. (I) Illustration of the fate of [2,3,3-^{2}H] serine involved in a one-carbon metabolism in the cytoplasmic pathway (blue) and mitochondrial pathway (red). (J) Relative content of intracellular [2,3,3-^{2}H] serine metabolites in infected and uninfected cells. (K) Relative abundance of [2,3,3-^{2}H] serine contributed to glycine (M + 1) in infected and uninfected cells. (L) Relative abundance of [2,3,3-^{2}H] serine contributed to cytosolic dTMP (M + 2) and mitochondria (M + 1) infected and uninfected cells. ns, not significant; *, $P < 0.05$; **, $P < 0.01$; ***, $P < 0.001$ by two-sample *t* test. Data are represented as the mean ± SD; $n = 3$ independent biological replicates.

mediated the activation of 1C metabolism; therefore, we examined the possible differential regulation of key enzymes of the mitochondrial and cytosolic pathways by NDV by collecting NDV-infected A549 cells at different times for analysis. As shown in Fig. 4A, the expression of SHMT1, MTHFD1L, and MTHFD2 was significantly higher in the infected group than in the uninfected group at the viral infection time points of 12 h and 18 h (Fig. 4B to D), whereas the expression levels of SHMT2 and MTHFD1 were not significantly different (Fig. 4E and F). Overall, NDV is involved in the regulation of 1C metabolism, and the upregulation of MTHFD2 and SHMT1 may be beneficial in alleviating the deficiency of *de novo* serine synthesis from the glycolysis pathway.

We examined the dependence of NDV replication on cytosolic SHMT1 and MTHFD1 versus mitochondrial SHMT2, MTHFD2, and MTHFD1L by determining extracellular viral titers and intracellular viral protein expression after knockdown of the indicated enzyme genes. Interestingly, except for cytosolic MTHFD1, NDV infection was suppressed in SHMT1-, SHMT2-, MTHFD1L-, and MTHFD2-knockdown cells, as indicated by the lower NDV NP expression and extracellular progeny production compared to the siNC group (Fig. 4G and H). Although SHMT1/2 act as compensatory reactions under some conditions (14), a loss of either reaction would inhibit NDV replication, and a similar situation was observed for cytosolic MTHFD1. Figure 4I illustrates the effect of knocking out the 1C metabolic pathway on NDV replication; loss of these pathways decreases the intracellular NADPH/NADP$^+$ ratio and suppresses nucleotide synthesis
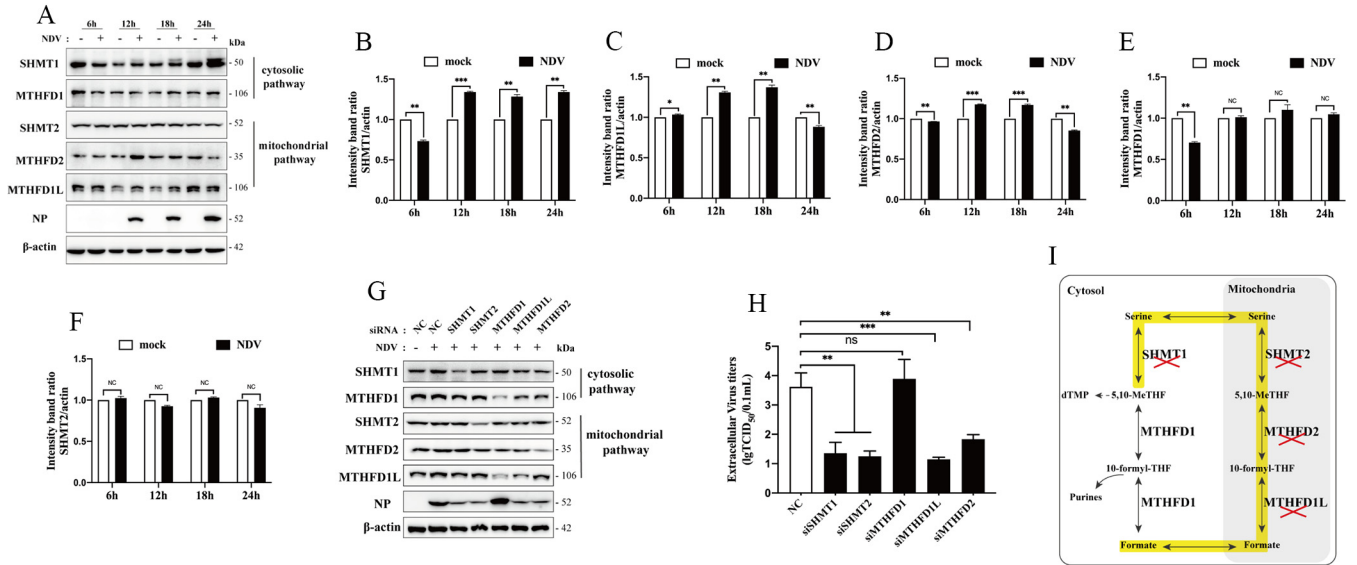
FIG 4 NDV replication depends on the folate-mediated one-carbon metabolic pathway except cytosolic MTHFD1. (A) Expression of one-carbon metabolic enzymes in NDV-infected A549 cells over the infection time. (B, C, D, E, and F) Intensity band ratios of the level of intracellular SHMT1, MTHFD1L, MTHFD2, MTHFD1, and SHMT2 to β-actin. (G) NDV NP protein expression was detected by siRNA interference with specific enzymes in the one-carbon metabolism pathway, including SHMT1, SHMT2, MTHFD1, MTHFD2, and MTHFD1L, respectively. (H) Cells treated with siRNA were infected with NDV, and the virus supernatant was collected at 12 h to determine the extracellular NDV titers in BHK-21 cells. Statistical analysis of $TCID_{50}$ was performed based on the Reed-Muench method. (I) Schematic showing that NDV was significantly inhibited in SHMT1-, SHMT2-, MTHFD1L-, and MTHFD2-deficient cells (yellow highlighting). ns, not significant; *, $P < 0.05$; **, $P < 0.01$; ***, $P < 0.001$ by a two-sample t test. Data are presented as the mean $\pm$ SD; $n = 3$ independent biological replicates.

(17, 28, 29). Taken together, these results suggest that NDV replication may be selectively dependent on 1C pathway enzymes and that it favors the mitochondrial 1C pathway.

Mitochondrial MTHFD2 modulates NDV replication by regulating nucleotide availability. One of the functions of the 1C metabolic pathway is to provide 1C units to sustain nucleotide synthesis. Exogenously supplied formate, as a precursor of *de novo* nucleotide synthesis, can increase the levels of intracellular nucleotides when the breakdown of serine is blocked (30, 31). Surprisingly, in this study, formate supplementation only rescued NDV replication after suppression of MTHFD2 by knockdown, but replication was not rescued by formate supplementation of SHMT1/2- and MTHFD1L-deficient cells (Fig. 5A and B). We also investigated the role of formate in rescuing viral replication following MTHFD2 knockdown by transfecting A549 cells with NC and siRNA targeting MTHFD2. Consistent with previous reports, MTHFD2 knockdown reduced the intracellular NADPH/NADP$^+$ ratio and increased the level of intracellular AICAR, an intermediate in the *de novo* purine synthesis pathway, thereby activating AMPK (17, 22). Figure 5C shows that MTHFD2 knockdown increased AICAR-induced AMPK phosphorylation; however, the increased AICAR may be consumed by NDV replication, so no AMPK activation was observed in the NDV-infected MTHFD2-deleted cells. Interestingly, the intracellular NADPH/NADP$^+$ ratio was significantly increased by formate supplementation in MTHFD2-knockdown cells, but not in the control group (Fig. 5D), similar to the response to RRx-001 (Fig. 2E and H). An increased NADPH/NADP$^+$ ratio facilitates the synthesis of nucleotide precursors (26). Taken together, these findings indicated that formate supplementation maintained the redox balance to support NDV replication by upregulating the NADPH/NADP$^+$ ratio.

We also explored the dependence of NDV replication on the 1C metabolic pathway by performing a series of targeted metabolic rescue experiments. NDV was inoculated into SHMT1/2- or MTHFD2/1L-deficient cells, and the cells were then supplemented with formate, adenine, uridine, or hypoxanthine. Figure 5E and F show that the inhibition of SHMT1/2 or MTHFD1L significantly reduced NDV NP protein expression even in the presence of exogenous nucleotides. These results suggest that NDV replication did not have a selective dependence on SHMT1/2 or MTHFD1L to facilitate nucleotide biosynthesis. A loss of redox homeostasis due to SHMT1/2
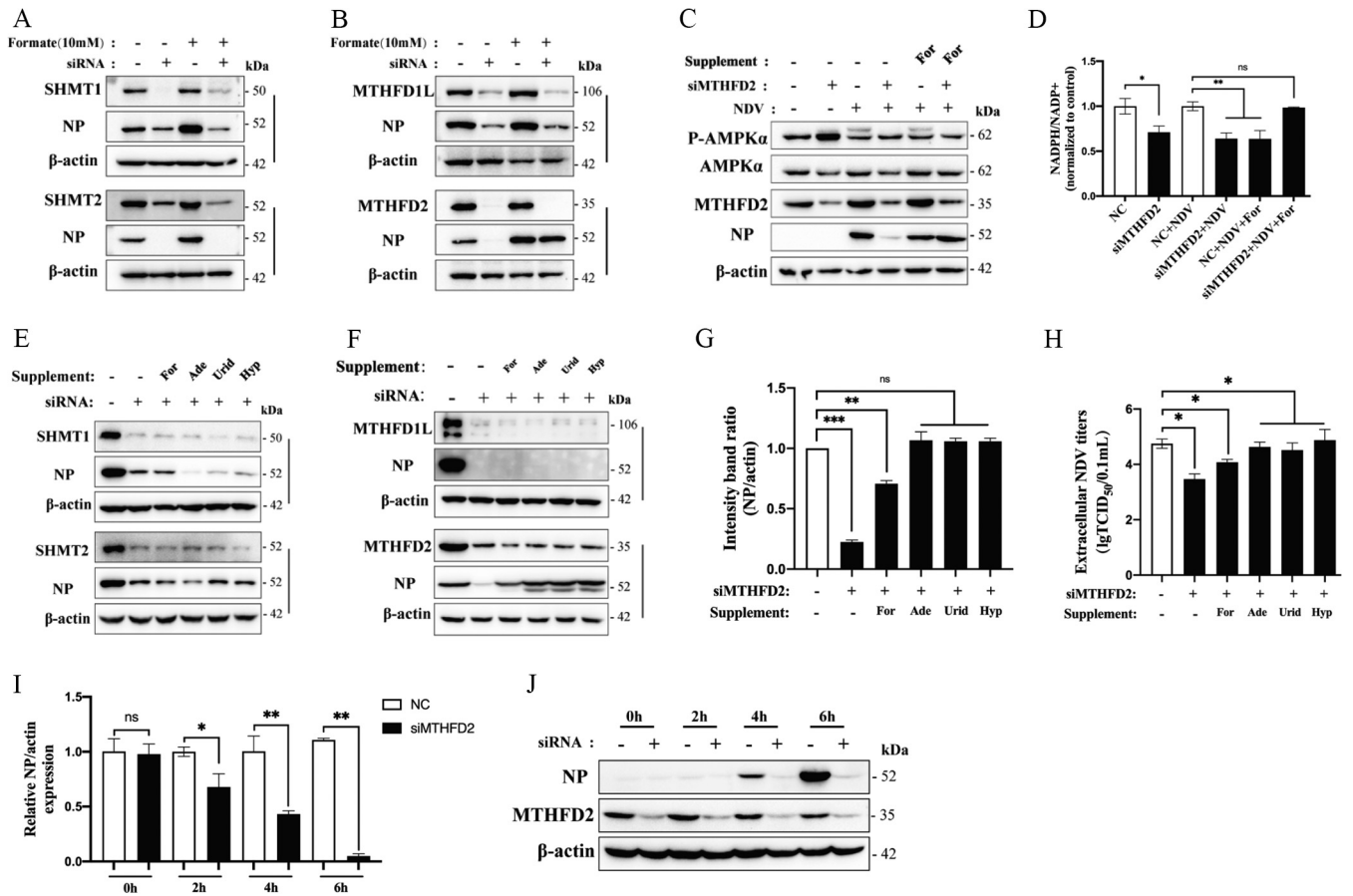
FIG 5 MTHFD2 functions as a regulatory target for NDV replication-dependent nucleotide synthesis. (A) Western blot analysis of NDV NP expression in infected cells treated with SHMT1/2 siRNA following treatment with or without formate. (B) NDV NP expression was measured in infected cells transfected with MTHFD1L/2 siRNA and cultured with or without formate. (C) AMPK and p-AMPK expression in NDV-infected MTHFD2-knockdown or normal cells treated with or without formate. (D) NDV-infected cells were transfected with control or MTHFD2 siRNA, and intracellular NADPH/NADP$^+$ ratios were determined after treatment with or without formate. (E) NDV replication in siSHMT1 or siSHMT2 cells was restored by the addition of formate (For), adenine (Ade), uridine (Urid), and hypoxanthine (Hyp). Western blots showing viral NP expression. (F) NDV NP expression was measured in infected cells transfected siRNA MTHFD1L/2 and cultured in unsupplemented media or media supplemented with formate (10 mM), adenine (50 μM), hypoxanthine (6 μM), or uridine (200 μM). Intensity band ratios of intracellular NP to β-actin (G) and the extracellular NDV titers (H) were measure after supplementation of NDV-infected MTHFD2-knockdown cells with formate or exogenous nucleotides. Effect of MTHFD2 knockdown on NDV adsorption by detection of NDV NP mRNA transcript levels (I) and protein levels (J). ns, not significant; *, $P < 0.05$; **, $P < 0.01$; ***, $P < 0.001$ by a two-sample t test. Data are presented as the mean $\pm$ SD; $n = 3$ independent biological replicates.

ablation may represent a major cause of restriction of viral replication (13, 32). The MTHFD2 deletion-mediated inhibition of NDV replication resulted in a marked rescue of intracellular NDV NP expression as well as extracellular viral titers by formate and exogenous nucleotides, as measured by 50% tissue culture infective dose (TCID$_{50}$) (Fig. 5F to H). However, the same result was not observed in Beas-2B cells (Fig. S1C). MTHFD2 knockdown did not affect the NDV adsorption process but instead inhibited postadsorption events, including significant suppression of NDV NP transcription and intracellular NDV NP expression (Fig. 5I and J). This indicates that the nucleotides required for NDV replication are regulated by mitochondrial MTHFD2. Thus, during NDV replication, the nucleotide synthesis driven by 1C metabolic pathways is regulated by mitochondrial MTHFD2.

Folate-mediated 1C metabolism-dependent NDV replication is regulated by c-Myc. The c-Myc transcriptional regulator had multiple targets (33, 34), including the mitochondrial 1C pathway (11, 18); however, direct regulation of SHMT1, SHMT2, MTHFD1L, and MTHFD2 protein expression by c-Myc in NDV-infected cells has not yet been reported. We used siRNA targeting c-Myc to evaluate whether c-Myc knockdown suppressed SHMT1, MTHFD2, and MTHFD1L protein expression in the presence or absence of NDV infection. Interestingly, c-Myc knockdown by siRNA significantly inhibited SHMT1, MTHFD1L, and
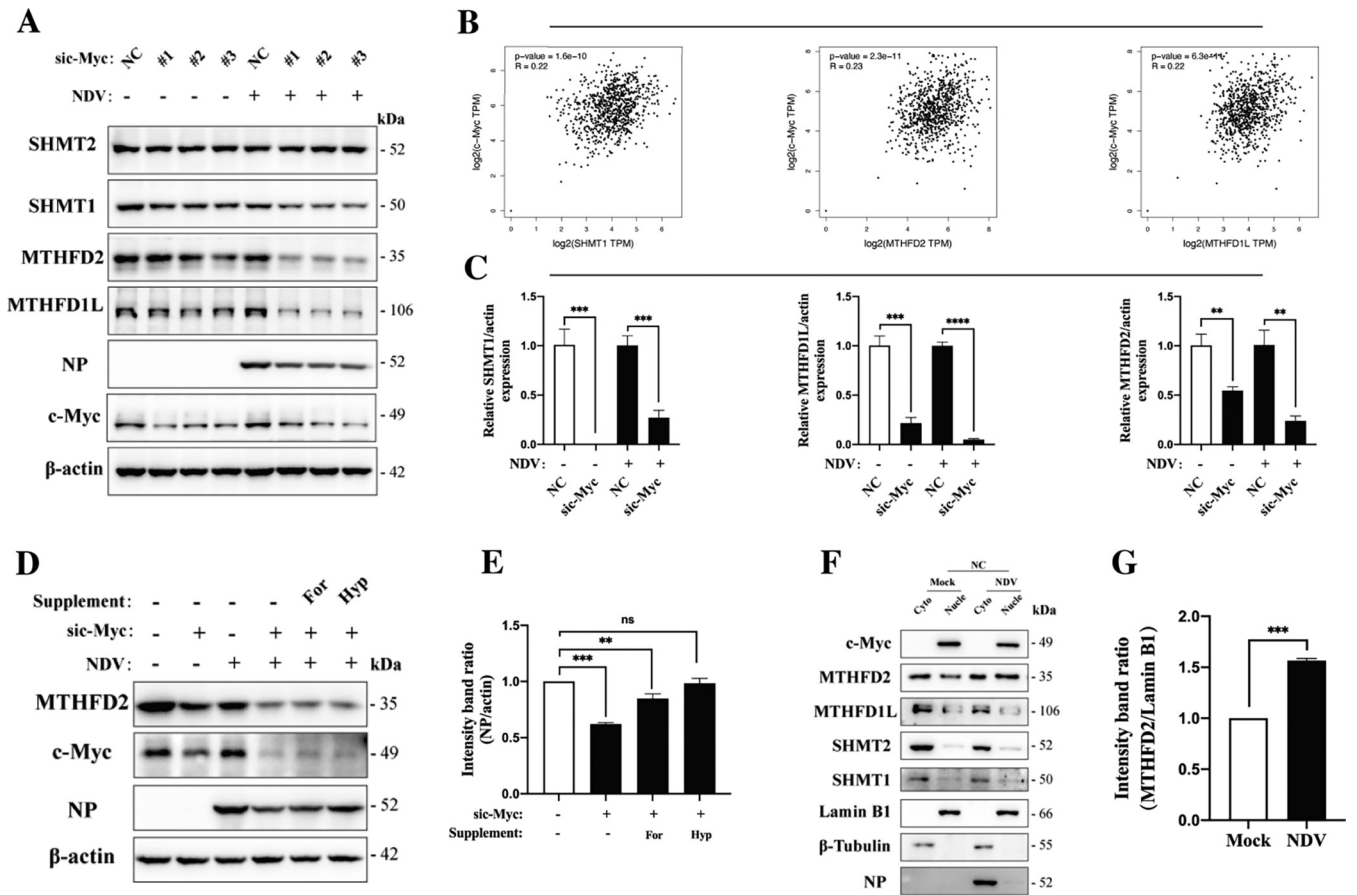
FIG 6 NDV infection increased MTHFD2 expression in the nucleus. (A) Immunoblot evaluation of the knockdown efficiency of c-Myc with three unique siRNAs and intracellular expression of one-carbon metabolic enzymes in noninfected and infected NDV cells. (B) Scatterplots of SHMT1, MTHFD2, MTHFD1L, and c-Myc expression was observed in LUAD tumor and LUAD normal groups based on data from the TCGA database on the GEPIA Platform (http://gepia .cancer-pku.cn/). (C) Intracellular transcript levels of SHMT1, MTHFD2, and MTHFD1L in c-Myc-knockdown cells with or without NDV infection. NC, negative control; sic-Myc, small interfering RNA c-Myc. (D) Western blot analysis of NDV NP protein expression after c-Myc knockdown and supplementation of formate and hypoxanthine. (E) Intensity band ratios of intracellular NP to β-actin. (F) Immunoblot analysis of MTHFD2 distribution in the cytosol and nucleus. Cells divided into nucleus and cytosol include NDV-infected and -uninfected. (G) Ratio of MTHFD2 to Lamin B1 intensity bands in the nucleus between infected and uninfected cells. ns, not significant; **, $P < 0.01$; ***, $P < 0.001$ by two-sample t test. Data are presented as the mean $\pm$ SD; $n = 3$ independent biological replicates.

MTHFD2 protein expression and inhibited NDV replication in NDV-infected cells (Fig. 6A). As shown in Fig. S1D to H, lung adenocarcinoma (LUAD) cells showed no differential expression of c-Myc but showed dramatic increases in cytoplasmic SHMT1 and mitochondrial MTHFD1L expression, and especially MTHFD2 (Fig. S1H). A correlation analysis by GEPIA 2, an online analysis platform derived from The Cancer Genome Atlas (TCGA) and Genotype-Tissue Expression (GTEx) databases, revealed a positive correlation between c-Myc expression and expression of SHMT1, MTHFD1L, and MTHFD2 in LUAD and normal lung tissues (Fig. 6B). Reverse transcriptase quantitative PCR (RT-qPCR) analysis showed lower transcription levels of SHMT1, MTHFD1L, and MTHFD2 in the c-Myc-knockdown tissues than in the NC group (Fig. 6C). These results may indicate that a loss of c-Myc can destabilize the MTHFD2 and MTHFD1L proteins in the mitochondrial 1C pathway, especially when disturbed by NDV infection. These data indicate that MTHFD2 inhibits viral replication by a mechanism that blocks nucleotide synthesis. We also confirmed that c-Myc inhibition of NDV replication involves the mitochondrial 1C pathway by showing that supplementation with either formate or hypoxanthine rescued the NDV replication that was inhibited by c-Myc deficiency (Fig. 6D and E). Collectively, these data suggest that a c-Myc deficiency restricts NDV replication by targeting nucleotide synthesis that depends on mitochondrial MTHFD2.

We also investigated why inhibition of NDV replication by c-Myc deficiency-mediated downregulation of mitochondrial MTHFD2 was rescued by exogenous nucleotides.

MTHFD2 is primarily localized in the mitochondria, but under certain conditions, it can also be found in the nucleus (19, 21). MTHFD2 binds to PARP3 in the nucleus to mediate DNA repair (35) or is associated with newly synthesized DNA (28). Therefore, we examined whether NDV infection might increase MTHFD2 expression in the nucleus to facilitate nucleotide synthesis by performing a nucleocytoplasmic separation of NDV-infected and -uninfected A549 cells and examined the localization of MTHFD2. Some MTHFD2 was localized in the cytoplasmic fraction (which included the mitochondria), but most of the MTHFD2 was found in the nucleus in the NDV-infected group (Fig. 6F and G). By contrast, SHMT1, SHMT2, and MTHFD1L were mainly localized in the cytoplasm, and their localization was not affected by NDV infection. Taken together, these findings suggest that NDV hijacks host cell nucleotides for its own replication by increasing MTHFD2 expression in the nucleus. These results further illustrate why exogenous nucleotides can rescue NDV replication only in cells with MTHFD2 knockdown of the mitochondrial 1C pathway.

DISCUSSION

In this study, we demonstrated that NDV replication depends on intracellular nucleotide availability, which is regulated by PPP and 1C metabolism. Drug inhibition experiments revealed that NDV hijacks the oxPPP to generate ribose for nucleotide synthesis and NADPH for antioxidant production and biosynthesis. NADPH, 1C units, and glycine from 1C metabolism are required for nucleotide synthesis and cellular proliferation (20) as well as for viral replication (36). Interestingly, MTHFD2 appears to function as a potential compensatory mechanism that can counteract the effects of serine deficiency on NDV replication. Furthermore, multifunctional proteins of the 1C metabolic pathway appear to perform different functions during the progression of NDV replication. Notably, NDV infection increased MTHFD2 expression associated with the mitochondrial 1C pathway only in the nucleus.

Glucose and its derived intermediate metabolites involved in nucleotide synthesis are hijacked by a variety of viruses to support viral replication (24, 37). We have previously reported the dependence of NDV replication on glucose metabolism (9). Interestingly, NDV infection increases glucose uptake and promotes R5P production via the oxPPP to maintain redox homeostasis and nucleotide synthesis. NADPH generated by the oxPPP is targeted by NDV to neutralize virus-produced ROS (6). Thus, treatment with NAC increased the NADPH/ $NADP^+$ ratio, thereby rescuing NDV replication in the presence of RRx-001. Moreover, the extent of NDV replication rescue was consistent with the levels of supplied exogenous nucleotides. NADPH availability contributes to biosynthesis, including nucleotide synthesis (6, 26), and 1C metabolism is a vital metabolic pathway that generates 1C units, glycine, and NADPH to drive nucleotide synthesis (11, 38). Serine, a nonessential amino acid, is catabolized to produce 1C metabolites that can be used for the production of nucleotides and NADPH via the cytosolic or mitochondrial 1C pathways (12, 22). In our present study, NDV infection did not increase the conversion of [1, 2-$^{13}C_2$] glucose to serine M + 2 by the glycolytic intermediate, 3-PG. Indeed, NDV replication did not depend on de novo serine synthesis but required increased uptake of extracellular serine. Similarly, proliferating cancer cells preferred exogenous serine, probably because switching the glycolytic pathway away from 3-PG to serine synthesis would interrupt glycolysis, thereby reducing energy production and mitochondrial oxidative phosphorylation (39). Most proliferating mammalian cells rely on the mitochondrial pathway to produce 1C units (22); therefore, the mitochondrial 1C pathway was selected by NDV for forming 1C units while simultaneously generating glycine and NADPH. Surprisingly, we first observed significant upregulation of mitochondrial MTHFD2 expression by NDV in response to insufficient serine availability in a viral infection model.

The folate-mediated 1C metabolic pathway achieves the biosynthesis of nucleotides and maintains the redox balance through both the cytosolic and mitochondrial pathways. Cytosolic SHMT1 and mitochondrial SHMT2 can convert serine to glycine and 5,10-methylene tetrahydrofolate to contribute to downstream metabolic pathways that directly replenish 1C pools or maintain redox balance, both of which are important for the cell cycle and cell proliferation (13, 40). Nevertheless, the hypothesis that

SHMT-driven nucleotide synthesis supports NDV replication is not valid. During NDV replication, SHMT1/2 may play other indispensable functions, including the maintenance of redox homeostasis. A similar situation has been observed for mitochondrial MTHFD1L, which contributes to the production and accumulation of NADPH to neutralize oxidative stress (28). In the mitochondrial 1C pathway, MTHFD2 is a bifunctional enzyme that generates antioxidant NADPH and 10-formyl-THF for subsequent purine synthesis by dehydrogenase and cyclohydrolase activities. MTHFD2 knockdown leads to the accumulation of the *de novo* purine synthesis intermediate, AICAR, which then activates AMPK (19), but this was reversed by NDV infection. Indeed, the inhibition of NDV replication by MTHFD2 knockdown was completely rescued by supplementation with exogenous nucleotides. However, this rescue of NDV replication by exogenous nucleotides was only observed in A549 cells after MTHFD2 suppression but not in Beas-2B normal lung cells. Compared with cancer cells, it may be that the plasticity of metabolic pathways is insufficient in normal cells, thereby reducing the possibility of NDV infection reshaping host metabolic pathways.

A recent report indicated that MTHFD2 preferentially binds to c-Myc at sites of new DNA synthesis in the nucleus (19, 21), thereby confirming MTHFD2 localization in the nucleus, where it presumably participates in the regulation of DNA synthesis. Therefore, increased nuclear MTHFD2 expression may be beneficial for nucleotide synthesis, and this makes our finding that NDV infection increased the level of MTHFD2 expression only in the nucleus particularly intriguing. This may be the reason why exogenous nucleotides can rescue NDV replication in of the presence of an MTHFD2 deficiency. Previous studies have shown that c-Myc knockdown can significantly decrease MTHFD2 transcription and protein levels (17, 18). Our results extend previous studies that showed an exacerbated inhibition of MTHFD2 expression by NDV infection of c-Myc-deficient cells. Moreover, nucleotide supplementation can also rescue NDV replication in c-Myc-deficient cells. Thus, our study provides a novel perspective on the targets of viral replication involving c-Myc-dependent regulation of mitochondrial 1C pathway.

In conclusion, our results demonstrate that the folate-mediated 1C metabolic pathways lose their plasticity and become vulnerable targets for NDV replication. During NDV replication, the virus selectively promotes the synthesis of R5P and 1C units by the oxPPP and mitochondrial 1C pathways, respectively. In addition, MTHFD2, as a potent c-Myc target, is upregulated in the nucleus to support nucleotide synthesis.

MATERIALS AND METHODS

Cells, reagents, virus, and antibodies. The A549, Beas-2B, and BHK-21 cell lines were purchased from the Cell Bank of the Shanghai Institute of Biochemistry and Cell Biology, Chinese Academy of Science (http://www.cellbank.org.cn). A549 and Beas-2B cells were maintained in RPMI 1640 medium supplemented with 10% fetal bovine serum (FBS) (ExCell Bio; FSP500). BHK-21 cells were cultured in Dulbecco's modified Eagle's medium (DMEM) supplemented with 10% FBS. Unless otherwise specified, all experiments were carried out on A549 cells. The Herts/33 NDV strain was provided by the China Institute of Veterinary Drug Control (Beijing, China). RRx-001 and NCT-503 were obtained from MedChem Express (MCE; catalog numbers HY-16438 and HY-101966, respectively). Sodium formate (Sigma-Aldrich; 71539) was used as an exogenous 1C metabolite to produce 10-formyltetrahydrofolate (10-FTHF). Uridine, adenine, and hypoxanthine were purchased from Sigma-Aldrich (U303, A2786, and H9636, respectively) as exogenous nucleotides. [1,2-^{13}C$_2$] glucose and [2,3,3-^{2}H] serine were purchased from Cambridge Isotope Laboratories, Inc. (CLM-504-1 and DLM-582-PK). Mouse monoclonal anti-NP was prepared in our laboratory. Anti-β-actin (66009-1-Ig), PHGDH (14719-1-AP), MTHFD1 (10794-1-AP), and c-Myc (67447-1-Ig) were purchased from Proteintech. Lamin B1 (ab16048) was purchased from Abcam. β-tubulin (AC021) was purchased from ABclonal. SHMT1 (number 80715), SHMT2 (number 33443), MTHFD1L (number 14998), and MTHFD2 (number 98116) were purchased from Cell Signaling Technology.

siRNA transfection. The siRNAs targeting human genes were transfected using Lipofectamine 2000 following the manufacturer's procedure (Thermo Fisher Scientific). Three chemically synthesized siRNA oligonucleotides of the c-Myc gene were obtained from Genpharma (Shanghai, China). The siRNA sequences were as follows: human c-Myc#1, 5'-GAGGAUAUCUGGAAGAAAUTT-3'; human c-Myc#2, 5'-CAAGGUAGUUAUCCUUAAAUTT-3'; human c-Myc#3, 5'-GACGAGAACAGUUGAAACATT-3'. The MTHFD1 (5'-GCAAAUAAGGGCGAGACUGAA-3') siRNA was designed online using the siRNA Wizard v3.1 software provided by InvivoGen. The following other siRNAs were used as previously reported: PHGDH (41), SHMT1 (42), SHMT2 (40), MTHFD2 (43), and MTHFD1L (28). As nontargeting controls, negative control siRNA (siNC) was used as a negative control throughout this study. The sequences used for the synthesis of these siRNAs were obtained from Genpharma (Genepharma Corporation, Shanghai, China).

Cells were seeded into six-well plates and reached 60% to 80% confluence within 24 h. Transfection

was conducted using an A/B tube method. Briefly, the A tube contained 5 μL Lipofectamine 2000 transfection reagent and 250 μL Opti-MEM. The B tube contained 10 μL siRNA (100 nM) and 250 μL Opti-MEM. After standing for 5 min at room temperature, the A and B tubes were mixed and allowed to stand for 15 min at room temperature. During this period, the cell plate was rinsed three times with phosphate-buffered saline (PBS), and 1.5 mL of Opti-MEM medium was added. At the end of the incubation period, the A/B mixture was added dropwise to the cells in the six-well plate, incubated in a cell incubator (37°C, 5% CO_2) for 4 to 6 h, and then replaced with fresh Opti-MEM medium. After continuous culture for 36 h, the cells were treated as required.

Viral infection, drug treatment, and virus adsorption. For NDV infection, cells were infected with NDV at a multiplicity of infection (MOI) of 1 in serum-free medium and incubated in a cell culture incubator for 1 h. The virus-containing supernatant was then replaced with maintenance medium containing 1% FBS. For the pharmacological experiments, an appropriate amount of drug was added to the maintenance medium according to the experimental design and cultured to the specified time point. The classical Reed-Muench method was used to measure the virus titer of the medium, using BHK-21 cells to determine the median tissue culture infective dose ($TCID_{50}$). The expression of NDV NP protein was measured by Western blotting as an indirect reflection of the level of virus replication. Cell samples were collected for metabolomics analysis, Western blotting, or NADPH/NADP$^+$ determinations.

For viral adsorption tests, cells were pretreated with RRx-001 for 3 h, and MTHFD2-knockdown cells were incubated at 4°C for 0.5 h. Cells were then infected with NDV at an MOI of 5 and incubated at 4°C for 1 h. After viral adsorption, the cells were washed 5 times with precooled PBS. Samples were collected at the 0 h point for adsorption determination, and the remaining cells were incubated in fresh maintenance medium containing 1% FBS and cultured at 37°C with 5% CO_2 in a humidified incubator. Cells were sampled at 2 h, 4 h, and 6 h and subjected to RT-qPCR and protein immunoblotting.

LC-MS metabolites analysis. Cells were seeded into 6-cm dishes and grown to approximately 90% confluence. Mock (uninfected) and NDV-infected cells were cultured for 12 h for metabolomics analysis. For [1,2-13C2]-labeled glucose treatments, after NDV infection, the culture medium in the control group was replaced with 12.5 mM [1,2-13C2] glucose and 12.5 mM nonlabeled glucose in DMEM. Cells for intracellular metabolite extraction were collected and washed twice with ice-cold PBS, and metabolites were frozen in liquid nitrogen to stop metabolic enzyme activity and extracted with ice-cold 80% LC-MS-grade methanol. The extracts were collected by vortexing and shaking for 15 min and centrifuging at 12,000 rpm (rpm) at 4°C for 15 min. The metabolites were vacuum freeze-dried in a CentriVap vacuum concentrator (Labconco Corporation, Kansas City, MO, USA). Positive and negative ionization mode data were collected using an AB SCIEX QTRAP 5500 mass spectrometer.

The [2,3,3-^{2}H]-labeled serine tracer experiments followed the protocol described by Yang et al. (12). For the extraction of cellular metabolites, briefly, hydride exchange was prevented by eliminating rinsing with PBS. The cells were frozen in liquid nitrogen and directly extracted with ice-cold acetonitrile-methanol-water (2:2:1, vol/vol) containing 0.5% formic acid and then immediately neutralized by adding 15% NH_4HCO_3. The subsequent steps were as described for the ^{13}C analyses.

RT-qPCR. Total RNA was extracted from the cell samples using traditional extraction methods and reverse transcribed using M-MLV reverse transcriptase (Promega; M1705). The RT-qPCR probes were obtained using SYBR green qPCR mix (GDSBio, Guangzhou Gongsheng Biotech Co., Ltd.; P2093). The primers targeting different genes were as follows: c-Myc (35), SHMT1 (44), MTHFD1L (45), and MTHFD2 (46). The NDV NP primer sequences were as follows: 5′-CAACAATAGGAGTGGAGTGTCTGA-3′ and downstream primer, 5′-CAGGGTATCG GTGATGTCTTCT-3′. All primer pairs were synthesized by Shanghai Sangon Biotech (Shanghai, China). All samples were standardized according to the mRNA level of β-actin.

Western blot analysis. Cell samples were washed with PBS and lysed by adding radioimmunoprecipitation assay (RIPA) lysis buffer (Beyotime; P0013C) (containing 1 mM phenylmethylsulfonyl fluoride [PMSF] [Beyotime, ST506]) with several blows and left at room temperature for 5 min. The cells were collected by scraping into 1.5-mL centrifuge tubes and centrifuging at 12,000 rpm for 5 min. The supernatant was mixed 5:1 with 5× sodium dodecyl sulfate-polyacrylamide gel electrophoresis (SDS-PAGE) sample loading buffer, boiled for 15 min, briefly centrifuged, and stored at −20°C for later use. Equal amounts of protein from the cell extracts were separated on 10% SDS-PAGE gels and transferred to a nitrocellulose blotting membrane (GE Healthcare Life Science, Amersham; Protran, 0.2 or 0.45 NC, Germany) by wet blotting. The membranes were then blocked with 5% skimmed milk in Tris-buffered saline containing 0.05% Tween 20 (TBST) and incubated for 1 h at room temperature. The membrane was washed to remove skim milk residues and incubated overnight at 4°C with the primary antibodies. After another wash, the membrane was incubated with secondary antibodies at room temperature for 2 h. After a further wash, the antibody-antigen complex was revealed with a LumiQ horseradish peroxidase (HRP) kit (Share-bio Biotechnology, Shanghai, China) and a multichemiluminescence image analysis system (Tanon 5200, Tanon, Guangzhou, China).

Intracellular NADP$^+$ and NADPH assay. Cell samples were washed with PBS, and the levels of intracellular NADP$^+$/NADPH were measured with an NADP$^+$/NADPH assay kit with WST-8 (Beyotime, S0179).

Gene expression correlation analysis. A gene expression correlation analysis between c-Myc and SHMT1, MTHFD2, and MTHFD1L was conducted using Gene Expression Profiling Interactive Analysis 2 (GEPIA 2) based on 483 tumor tissue samples, 59 normal tissue samples from the TCGA database, and 288 tissue samples from the GTEx database (47). These data were calculated using the non-log scale and visualized using the log scale axis.

Statistical analysis. Data represent the means of at least three independent experiments. Statistical analysis was performed using GraphPad Prism software 9.0 (GraphPad Software, Inc.), and all results are presented as the mean $\pm$ standard error of the mean (SEM). Statistical significance was evaluated with

an unpaired Student's *t* test. A *P* value of <0.05 was considered statistically significant. ns, *P* > 0.05; *, *P* < 0.05; **, *P* < 0.01; ***, *P* < 0.001.

SUPPLEMENTAL MATERIAL

Supplemental material is available online only.

SUPPLEMENTAL FILE 1, PDF file, 0.2 MB.

REFERENCES

1. Todo T, Ito H, Ino Y, Ohtsu H, Ota Y, Shibahara J, Tanaka M. 2022. Intratumoral oncolytic herpes virus G47Δ for residual or recurrent glioblastoma: a phase 2 trial. Nat Med 28:1630–1639. https://doi.org/10.1038/s41591-022-01897-x.
2. Naik JD, Twelves CJ, Selby PJ, Vile RG, Chester JD. 2011. Immune recruitment and therapeutic synergy: keys to optimizing oncolytic viral therapy? Clin Cancer Res 17:4214–4224. https://doi.org/10.1158/1078-0432.CCR-10-2848.
3. Nishimura T, Nakata A, Chen X, Nishi K, Meguro-Horike M, Sasaki S, Kita K, Horike S-I, Saitoh K, Kato K, Igarashi K, Murayama T, Kohno S, Takahashi C, Mukaida N, Yano S, Soga T, Tojo A, Gotoh N. 2019. Cancer stem-like properties and gefitinib resistance are dependent on purine synthetic metabolism mediated by the mitochondrial enzyme MTHFD2. Oncogene 38:2464–2481. https://doi.org/10.1038/s41388-018-0589-1.
4. Tate PM, Mastrodomenico V, Mounce BC. 2019. Ribavirin induces polyamine depletion via nucleotide depletion to limit virus replication. Cell Rep 28:2620–2633. https://doi.org/10.1016/j.celrep.2019.07.099.
5. Anderson CL, Sullivan MB, Fernando SC. 2017. Dietary energy drives the dynamic response of bovine rumen viral communities. Microbiome 5:155. https://doi.org/10.1186/s40168-017-0374-3.
6. Fan J, Ye J, Kamphorst JJ, Shlomi T, Thompson CB, Rabinowitz JD. 2014. Quantitative flux analysis reveals folate-dependent NADPH production. Nature 510:298–302. https://doi.org/10.1038/nature13236.
7. Li Q, Qin T, Bi Z, Hong H, Ding L, Chen J, Wu W, Lin X, Fu W, Zheng F, Yao Y, Luo M-L, Saw PE, Wulf GM, Xu X, Song E, Yao H, Hu H. 2020. Rac1 activates non-oxidative pentose phosphate pathway to induce chemoresistance of breast cancer. Nat Commun 11:1456. https://doi.org/10.1038/s41467-020-15308-7.
8. Li Y, Yao C-F, Xu F-J, Qu Y-Y, Li J-T, Lin Y, Cao Z-L, Lin P-C, Xu W, Zhao S-M, Zhao J-Y. 2019. APC/CCDH1 synchronizes ribose-5-phosphate levels and DNA synthesis to cell cycle progression. Nat Commun 10:2502. https://doi.org/10.1038/s41467-019-10375-x.
9. Gong Y, Tang N, Liu P, Sun Y, Lu S, Liu W, Tan L, Song C, Qiu X, Liao Y, Yu S, Liu X, Lin S-H, Ding C. 2022. Newcastle disease virus degrades SIRT3 via PINK1-PRKN-dependent mitophagy to reprogram energy metabolism in infected cells. Autophagy 18:1503–1521. https://doi.org/10.1080/15548627.2021.1990515.
10. Passalacqua KD, Lu J, Goodfellow I, Kolawole AO, Arche JR, Maddox RJ, Carnahan KE, O'Riordan MXD, Wobus CE. 2019. Glycolysis is an intrinsic factor for optimal replication of a norovirus. mBio 10:e02175-18. https://doi.org/10.1128/mBio.02175-18.
11. Wang LW, Shen H, Nobre L, Ersing I, Paulo JA, Trudeau S, Wang Z, Smith NA, Ma Y, Reinstadler B, Nomburg J, Sommermann T, Cahir-McFarland E, Gygi SP, Mootha VK, Weekes MP, Gewurz BE. 2019. Epstein-Barr-virus-induced one-carbon metabolism drives B cell transformation. Cell Metab 30:539–555. https://doi.org/10.1016/j.cmet.2019.06.003.
12. Yang L, Garcia Canaveras JC, Chen Z, Wang L, Liang L, Jang C, Mayr JA, Zhang Z, Ghergurovich JM, Zhan L, Joshi S, Hu Z, McReynolds MR, Su X, White E, Morscher RJ, Rabinowitz JD. 2020. Serine catabolism feeds NADH when respiration is impaired. Cell Metab 31:809–821. https://doi.org/10.1016/j.cmet.2020.02.017.
13. Dou C, Xu Q, Liu J, Wang Y, Zhou Z, Yao W, Jiang K, Cheng J, Zhang C, Tu K. 2019. SHMT1 inhibits the metastasis of HCC by repressing NOX1-mediated ROS production. J Exp Clin Cancer Res 38:70. https://doi.org/10.1186/s13046-019-1067-5.
14. Pan C, Li B, Simon MC. 2021. Moonlighting functions of metabolic enzymes and metabolites in cancer. Mol Cell 81:3760–3774. https://doi.org/10.1016/j.molcel.2021.08.031.
15. Ron-Harel N, Santos D, Ghergurovich JM, Sage PT, Reddy A, Lovitch SB, Dephoure N, Satterstrom FK, Sheffer M, Spinelli JB, Gygi S, Rabinowitz JD, Sharpe AH, Haigis MC. 2016. Mitochondrial biogenesis and proteome remodeling promote one-carbon metabolism for T cell activation. Cell Metab 24:104–117. https://doi.org/10.1016/j.cmet.2016.06.007.
16. Anderson DE, Cui J, Ye Q, Huang B, Tan Y, Jiang C, Zu W, Gong J, Liu W, Kim SY, Yan BG, Sigmundsson K, Lim XF, Ye F, Niu P, Irving AT, Zhang H, Tang Y, Zhou X, Wang Y, Tan W, Wang L-F, Tan X. 2021. Orthogonal genome-wide screens of bat cells identify MTHFD1 as a target of broad antiviral therapy. Proc Natl Acad Sci U S A 118:e2104759118. https://doi.org/10.1073/pnas.2104759118.
17. Ju H-Q, Lu Y-X, Chen D-L, Zuo Z-X, Liu Z-X, Wu Q-N, Mo H-Y, Wang Z-X, Wang D-S, Pu H-Y, Zeng Z-L, Li B, Xie D, Huang P, Hung M-C, Chiao PJ, Xu R-H. 2019. Modulation of redox homeostasis by inhibition of MTHFD2 in colorectal cancer: mechanisms and therapeutic implications. J Natl Cancer Inst 111:584–596. https://doi.org/10.1093/jnci/djy160.
18. Pikman Y, Puissant A, Alexe G, Furman A, Chen LM, Frumm SM, Ross L, Fenouille N, Bassil CF, Lewis CA, Ramos A, Gould J, Stone RM, DeAngelo DJ, Galinsky I, Clish CB, Kung AL, Hemann MT, Vander Heiden MG, Banerji V, Stegmaier K. 2016. Targeting MTHFD2 in acute myeloid leukemia. J Exp Med 213:1285–1306. https://doi.org/10.1084/jem.20151574.
19. Li G, Wu J, Li L, Jiang P. 2021. p53 deficiency induces MTHFD2 transcription to promote cell proliferation and restrain DNA damage. Proc Natl Acad Sci U S A 118:e2019822118. https://doi.org/10.1073/pnas.2019822118.
20. Ye J, Fan J, Venneti S, Wan Y-W, Pawel BR, Zhang J, Finley LWS, Lu C, Lindsten T, Cross J, Qing G, Liu Z, Simon MC, Rabinowitz JD, Thompson CB. 2014. Serine catabolism regulates mitochondrial redox control during hypoxia. Cancer Discov 4:1406–1417. https://doi.org/10.1158/2159-8290.CD-14-0250.
21. Gustafsson Sheppard N, Jarl L, Mahadessian D, Strittmatter L, Schmidt A, Madhusudan N, Tegnér J, Lundberg EK, Asplund A, Jain M, Nilsson R. 2015. The folate-coupled enzyme MTHFD2 is a nuclear protein and promotes cell proliferation. Sci Rep 5:15029. https://doi.org/10.1038/srep15029.
22. Ducker GS, Chen L, Morscher RJ, Ghergurovich JM, Esposito M, Teng X, Kang Y, Rabinowitz JD. 2016. Reversal of cytosolic one-carbon flux compensates for loss of the mitochondrial folate pathway. Cell Metab 23:1140–1153. https://doi.org/10.1016/j.cmet.2016.04.016.
23. Oslund RC, Su X, Haugbro M, Kee J-M, Esposito M, David Y, Wang B, Ge E, Perlman DH, Kang Y, Muir TW, Rabinowitz JD. 2017. Bisphosphoglycerate mutase controls serine pathway flux via 3-phosphoglycerate. Nat Chem Biol 13:1081–1087. https://doi.org/10.1038/nchembio.2453.
24. Eisenreich W, Rudel T, Heesemann J, Goebel W. 2019. How viral and intracellular bacterial pathogens reprogram the metabolism of host cells to allow

their intracellular replication. Front Cell Infect Microbiol 9:42. https://doi.org/10.3389/fcimb.2019.00042.

25. Cosentino C, Grieco D, Costanzo V. 2011. ATM activates the pentose phosphate pathway promoting anti-oxidant defence and DNA repair. EMBO J 30:546–555. https://doi.org/10.1038/emboj.2010.330.

26. Zhang Y, Xu Y, Lu W, Ghergurovich JM, Guo L, Blair IA, Rabinowitz JD, Yang X. 2021. Upregulation of antioxidant capacity and nucleotide precursor availability suffices for oncogenic transformation. Cell Metab 33:94–109. https://doi.org/10.1016/j.cmet.2020.10.002.

27. Labuschagne CF, van den Broek NJF, Mackay GM, Vousden KH, Maddocks ODK. 2014. Serine, but not glycine, supports one-carbon metabolism and proliferation of cancer cells. Cell Rep 7:1248–1258. https://doi.org/10.1016/j.celrep.2014.04.045.

28. Lee D, Xu IM-J, Chiu DK-C, Lai RK-H, Tse AP-W, Lan Li L, Law C-T, Tsang FH-C, Wei LL, Chan CY-K, Wong C-M, Ng IO-L, Wong CC-L. 2017. Folate cycle enzyme MTHFD1L confers metabolic advantages in hepatocellular carcinoma. J Clin Invest 127:1856–1872. https://doi.org/10.1172/JCI90253.

29. Tajan M, Hennequart M, Cheung EC, Zani F, Hock AK, Legrave N, Maddocks ODK, Ridgway RA, Athineos D, Suárez-Bonnet A, Ludwig RL, Novellasdemunt L, Angelis N, Li VSW, Vlachogiannis G, Valeri N, Mainolfi N, Suri V, Friedman A, Manfredi M, Blyth K, Sansom OJ, Vousden KH. 2021. Serine synthesis pathway inhibition cooperates with dietary serine and glycine limitation for cancer therapy. Nat Commun 12:366. https://doi.org/10.1038/s41467-020-20223-y.

30. Bao XR, Ong S-E, Goldberger O, Peng J, Sharma R, Thompson DA, Vafai SB, Cox AG, Marutani E, Ichinose F, Goessling W, Regev A, Carr SA, Clish CB, Mootha VK. 2016. Mitochondrial dysfunction remodels one-carbon metabolism in human cells. Elife 5:e10575. https://doi.org/10.7554/eLife.10575.

31. Oizel K, Tait-Mulder J, Fernandez-de-Cossio-Diaz J, Pietzke M, Brunton H, Lilla S, Dhayade S, Athineos D, Blanco GR, Sumpton D, Mackay GM, Blyth K, Zanivan SR, Meiser J, Vazquez A. 2020. Formate induces a metabolic switch in nucleotide and energy metabolism. Cell Death Dis 11:310. https://doi.org/10.1038/s41419-020-2523-z.

32. Lewis CA, Parker SJ, Fiske BP, McCloskey D, Gui DY, Green CR, Vokes NI, Feist AM, Vander Heiden MG, Metallo CM. 2014. Tracing compartmentalized NADPH metabolism in the cytosol and mitochondria of mammalian cells. Mol Cell 55:253–263. https://doi.org/10.1016/j.molcel.2014.05.008.

33. Salmanidis M, Brumatti G, Narayan N, Green BD, van den Bergen JA, Sandow JJ, Bert AG, Silke N, Sladic R, Puthalakath H, Rohrbeck L, Okamoto T, Bouillet P, Herold MJ, Goodall GJ, Jabbour AM, Ekert PG. 2013. Hoxb8 regulates expression of microRNAs to control cell death and differentiation. Cell Death Differ 20:1370–1380. https://doi.org/10.1038/cdd.2013.92.

34. Morelli E, Biamonte L, Federico C, Amodio N, Di Martino MT, Gallo Cantafio ME, Manzoni M, Scionti F, Samur MK, Gullà A, Stamato MA, Pitari MR, Caracciolo D, Sesti S, Frandsen NM, Rossi M, Neri A, Fulciniti M, Munshi NC, Tagliaferri P, Tassone P. 2018. Therapeutic vulnerability of multiple myeloma to MIR17PTi, a first-in-class inhibitor of pri-miR-17-92. Blood 132:1050–1063. https://doi.org/10.1182/blood-2018-03-836601.

35. Kato S, Akagi T, Sugimura K, Kishida A, Akashi M. 2000. Evaluation of biological responses to polymeric biomaterials by RT-PCR analysis IV: study of c-

myc, c-fos and p53 mRNA expression. Biomaterials 21:521–527. https://doi.org/10.1016/s0142-9612(99)00214-8.

36. Bojkova D, Klann K, Koch B, Widera M, Krause D, Ciesek S, Cinatl J, Münch C. 2020. Proteomics of SARS-CoV-2-infected host cells reveals therapy targets. Nature 583:469–472. https://doi.org/10.1038/s41586-020-2332-7.

37. Thai M, Graham NA, Braas D, Nehil M, Komisopoulou E, Kurdistani SK, McCormick F, Graeber TG, Christofk HR. 2014. Adenovirus E4ORF1-induced MYC activation promotes host cell anabolic glucose metabolism and virus replication. Cell Metab 19:694–701. https://doi.org/10.1016/j.cmet.2014.03.009.

38. Jain M, Nilsson R, Sharma S, Madhusudhan N, Kitami T, Souza AL, Kafri R, Kirschner MW, Clish CB, Mootha VK. 2012. Metabolite profiling identifies a key role for glycine in rapid cancer cell proliferation. Science 336:1040–1044. https://doi.org/10.1126/science.1218595.

39. Gravel S-P, Hulea L, Toban N, Birman E, Blouin M-J, Zakikhani M, Zhao Y, Topisirovic I, St-Pierre J, Pollak M. 2014. Serine deprivation enhances antineoplastic activity of biguanides. Cancer Res 74:7521–7533. https://doi.org/10.1158/0008-5472.CAN-14-2643-T.

40. Paone A, Marani M, Fiascarelli A, Rinaldo S, Giardina G, Contestabile R, Paiardini A, Cutruzzolà F. 2014. SHMT1 knockdown induces apoptosis in lung cancer cells by causing uracil misincorporation. Cell Death Dis 5:e1525. https://doi.org/10.1038/cddis.2014.482.

41. Dong J-K, Lei H-M, Liang Q, Tang Y-B, Zhou Y, Wang Y, Zhang S, Li W-B, Tong Y, Zhuang G, Zhang L, Chen H-Z, Zhu L, Shen Y. 2018. Overcoming erlotinib resistance in EGFR mutation-positive lung adenocarcinomas through repression of phosphoglycerate dehydrogenase. Theranostics 8:1808–1823. https://doi.org/10.7150/thno.23177.

42. Pandey S, Garg P, Lee S, Choung H-W, Choung Y-H, Choung P-H, Chung JH. 2014. Nucleotide biosynthesis arrest by silencing SHMT1 function via vitamin B6-coupled vector and effects on tumor growth inhibition. Biomaterials 35:9332–9342. https://doi.org/10.1016/j.biomaterials.2014.07.045.

43. Nilsson R, Jain M, Madhusudhan N, Sheppard NG, Strittmatter L, Kampf C, Huang J, Asplund A, Mootha VK. 2014. Metabolic enzyme expression highlights a key role for MTHFD2 and the mitochondrial folate pathway in cancer. Nat Commun 5:3128. https://doi.org/10.1038/ncomms4128.

44. Ding J, Li T, Wang X, Zhao E, Choi J-H, Yang L, Zha Y, Dong Z, Huang S, Asara JM, Cui H, Ding H-F. 2013. The histone H3 methyltransferase G9A epigenetically activates the serine-glycine synthesis pathway to sustain cancer cell survival and proliferation. Cell Metab 18:896–907. https://doi.org/10.1016/j.cmet.2013.11.004.

45. Yang J, Xu Q-C, Wang Z-Y, Lu X, Pan L-K, Wu J, Wang C. 2021. Integrated analysis of an lncRNA-associated ceRNA network reveals potential biomarkers for hepatocellular carcinoma. J Comput Biol 28:330–344. https://doi.org/10.1089/cmb.2019.0250.

46. Yu C, Yang L, Cai M, Zhou F, Xiao S, Li Y, Wan T, Cheng D, Wang L, Zhao C, Huang X. 2020. Down-regulation of MTHFD2 inhibits NSCLC progression by suppressing cycle-related genes. J Cell Mol Med 24:1568–1577. https://doi.org/10.1111/jcmm.14844.

47. Tang Z, Li C, Kang B, Gao G, Li C, Zhang Z. 2017. GEPIA: a web server for cancer and normal gene expression profiling and interactive analyses. Nucleic Acids Res 45:W98–W102. https://doi.org/10.1093/nar/gkx247.